DEUTSCHES ELEKTRONEN-SYNCHROTRON **DESY**

DESY 85-033
April 1985

A MEASUREMENT OF THE η RADIATIVE WIDTH $\Gamma_{\eta\to\gamma\gamma}$

by

JADE Collaboration

ISSN 0418-9833

NOTKESTRASSE 85 · 2 HAMBURG 52

To be sure that your preprints are promptly included in the
HIGH ENERGY PHYSICS INDEX ,
send them to the following address (if possible by air mail) :

DESY
Bibliothek
Notkestrasse 85
2 Hamburg 52
Germany

DESY 85-033
April 1985

ISSN 0418-9833

A measurement of the η radiative width $\Gamma_{\eta\to\gamma\gamma}$.

JADE Collaboration

W. Bartel, L. Becker, D. Cords[1], R. Felst, D. Haidt, H. Junge[2], G. Knies, H. Krehbiel, P. Laurikainen[3], R. Meinke, B. Naroska, J. Olsson, D. Schmidt[4], P. Steffen[5]
Deutsches Elektronen-Synchrotron DESY, Hamburg, Germany

G. Dietrich, J. Hagemann, G. Heinzelmann, H. Kado, K. Kawagoe[6], C. Kleinwort, M. Kuhlen, K. Meier[5], A. Petersen[1], R. Ramcke, U. Schneekloth, G. Weber
II Institut für Experimentalphysik der Universität Hamburg, Germany

K. Ambrus, S. Bethke, A. Dieckmann, E. Elsen, J. Heintze, K.-H. Hellenbrand, S. Komamiya, J. von Krogh, P. Lennert, H. Matsumura, H. Rieseberg, J. Spitzer, A. Wagner
Physikalisches Institut der Universität Heidelberg, Germany

C. Bowdery, A. Finch, F. Foster, G. Hughes, T. Nozaki[7], J. Nye
University of Lancaster, England

J. Allison, J. Baines, A.H. Ball[8], R.J. Barlow, J. Chrin, I.P. Duerdoth, T. Greenshaw, P. Hill, F.K. Loebinger, A.A. Macbeth, H. McCann, H.E. Mills, P.G. Murphy, K. Stephens, P. Warming
University of Manchester, England

R.G. Glasser, B. Sechi-Zorn[9], J.A.J. Skard, S.R. Wagner, G.T. Zorn
University of Maryland, College Park, Maryland, USA

S.L. Cartwright, D. Clarke, R. Marshall, R.P. Middleton, J.B. Whittaker
Rutherford Appleton Laboratory, Chilton, England

T. Kawamoto, T. Kobayashi, T. Mashimo, M. Minowa, H. Takeda, T. Takeshita, S. Yamada
Intern. Center for Elementary Particle Physics, University of Tokyo, Japan

[1] Now at SLAC, California, USA
[2] Now at Krupp Atlas Elektronik, Bremen, Germany
[3] University of Helsinki, Helsinki, Finland
[4] Universität-Gesamthochschule Wuppertal, Germany
[5] Now at CERN, Geneva, Switzerland
[6] Deutscher Akademischer Austauschdienst (DAAD) Fellow
[7] Now at KEK, Ibaraki, Japan
[8] Now at University of Maryland, USA
[9] Deceased

We wish to dedicate this letter to our friend Bice Sechi-Zorn who contributed so much to this work.

Abstract

The radiative width of the η meson has been measured at PETRA in photon-photon collisions. The resulting value is

$$\Gamma_{\eta\to\gamma\gamma} = 0.53 \pm 0.04 \pm 0.04 \text{ keV}.$$

The decay widths into two photons of the mesons π^0, $\eta(548)$ and $\eta'(958)$ are of considerable interest. They can be related to the well known questions of quark content and octet-singlet mixing in the pseudoscalar nonet[1], as well as to the fundamental question of fractional or integer quark charges[2]. They are also of importance for the discussion of a gluonic admixture in the pseudoscalar mesons and their relation to the pseudoscalar glueball candidate, $\iota(1440)$[3].

The radiative width $\Gamma_{\pi^0\to\gamma\gamma}$ is very accurately determined[4] and many measurements of $\Gamma_{\eta'\to\gamma\gamma}$ have recently been presented[5]. Relatively few measurements of $\Gamma_{\eta\to\gamma\gamma}$ have been made, however. The early measurements[6] which used the Primakoff effect[7] in photoproduction differ considerably from each other, and a recent measurement[8] which was obtained from $\gamma\gamma$ production of η in e^+e^- collisions, does not allow a definite conclusion.

We present in this letter a new measurement of $\Gamma_{\eta\to\gamma\gamma}$, where the η mesons were produced via the reaction

$$e^+e^- \to e^+e^-\eta, \qquad \eta \to \gamma\gamma. \tag{1}$$

The e^+ and e^- beam particles were scattered at small angles and were not detected. Thus the only detected particles from this reaction were the two photons from the η decay.

The experiment was performed at the e^+e^- storage ring PETRA, at a beam energy of 17.3 GeV. The detector used was JADE, a general purpose, large solid angle, charged particle and photon detector operating with a magnetic field of 0.48 tesla. Detailed descriptions of JADE appear in Ref. 9. In this experiment, photon detection was of particular importance. Photons were detected by an array of 2712 lead glass counters located outside of the central jet chamber and the magnet coil. They furnish complete azimuthal (ϕ) coverage over a θ range given by $|\cos\theta| < 0.82$ for the central barrel and $0.89 < |\cos\theta| < 0.97$ for the end caps, where θ is measured relative to the e^+ beam. The barrel consists of 30 rings, each with 84 counters. A single counter subtends $\sim 4°$ in azimuth.

A special trigger was set up for the detection of reaction (1) and other exclusive $\gamma\gamma$ reactions. The lead glass barrel counters were grouped in azimuth, ϕ, into seven sectors (henceforth called septants) and the linear analogue sum of the pulse-heights of the 360 counters in each septant was used to generate a septant signal. For the trigger, a coincidence was required between two septants, separated by at least two other septants, with all Time-Of-Flight (TOF) scintillation counters in anticoincidence. A maximum of three septant signals was allowed. The signal threshold for triggering was at two levels, Low Threshold (Run I) and High Threshold (Run II). Fig. 1 shows the linear sum trigger signal efficiency as a function of measured energy in septants for the Low and the High Thresholds. These curves were obtained from event samples selected using other, independent triggers. The chosen thresholds are below the typical deposited energy of 0.15 - 0.30 GeV for photons from reaction (1).

Events were required to satisfy the criteria described below:

i) Two and only two photons should be detected in the lead glass barrel and no other photons in the endcaps. This selection used a cluster algorithm which chose acceptable photon signals. The detection thresholds were 0.045 Gev for a single counter and 0.060 GeV for a cluster of adjacent counters. These detection thresholds were determined by the electronics readout threshold, which was 0.025 - 0.030 GeV for each counter.

ii) No charged particles should be detected in the jet chamber by the pattern recognition program.

iii) Events with penetrating cosmic ray muons, detected in the external muon chambers covering 92 % of the total solid angle, were rejected.

iv) The remaining cosmic ray muons which traversed the lead glass array but not the jet chamber were rejected by excluding events in which both photons had $|\cos\theta| > 0.68$[1] and where $\cos\theta_1 \cdot \cos\theta_2 > 0$.

[1]Here, as well as in the invariant mass calculation, the event vertex is taken to be the center of the detector, which coincides closely with the average e^+e^- collision point.

v) The acoplanarity angle $\Delta\phi$, defined as the smallest angle between the planes formed by each photon position and the beam line, was required to be smaller than 20°. This restricted the event sample to an angular region favoured by reaction (1), as shown below.

vi) Both photons in an event were required to have energies above 0.140 GeV and below 3 GeV. The latter restriction was imposed in order to exclude events from the QED reaction $e^+e^- \to \gamma\gamma$.

vii) All remaining events were visually inspected and events were eliminated if evidence of any charged particle track was seen in the jet chamber.

viii) The observed transverse momentum of the $\gamma\gamma$ system, $|\vec{p}_\perp|$, relative to the e^+e^- beam directions, was required to be smaller than 0.120 GeV/c. This cut serves to decrease background from beam-gas reactions as well as from other $\gamma\gamma$ reactions with additional, undetected final-state particles. It also limits the momentum transfer (q^2) of the virtual photons in reaction (1) to $|q^2| < 0.04$ $(\mathrm{GeV/c})^2$, with a mean $< q^2 > \cong -2 \cdot 10^{-4}$ $(\mathrm{GeV/c})^2$. The $p_\perp^2$ distribution for the events of Run I and II summed together is shown in Fig. 2. The $p_\perp^2$ limit is indicated by an arrow.

For the purpose of beam-gas background estimation, a third data sample, obtained in a run with the Low Threshold condition with separated e^+e^- beams (Run III), was subjected to the same selection criteria. The numbers of events remaining after all of the above restrictions for each of the samples are listed in Table 1.

The $\gamma\gamma$ invariant mass spectrum of the 1473 selected events from Run I and II is shown as a solid line histogram in Fig. 3. The distribution shows a clear peak in the η mass region. In addition to reaction (1), also other exclusive $\gamma\gamma$ reactions may contribute to this mass spectrum. The following reactions were considered:

$$\begin{array}{lll} e^+e^- \to e^+e^-\eta'; & \eta' \to \pi^+\pi^-\eta,\ \pi^0\pi^0\eta,\ \gamma\gamma; & \eta \to \gamma\gamma \\ e^+e^- \to e^+e^- f; & f \to \pi^0\pi^0 & \\ e^+e^- \to e^+e^- A_2; & A_2 \to \eta\pi^0; & \eta \to \gamma\gamma \end{array} \qquad (2)$$

With the exception of the decay $\eta' \to \gamma\gamma$, events from reactions (2) are incompletely measured and constitute a background to reaction (1). Also beam-gas reactions contribute. The mass spectrum of the 30 events in the separated beam data sample is also shown in Fig. 3 (solid histogram). These events contribute only in the mass region below 0.8 $\mathrm{GeV/c^2}$.

In order to evaluate the contribution of reaction (1) to the mass spectrum of Fig. 3 we will use the acoplanarity, $\Delta\phi$, for events with $\gamma\gamma$ invariant mass < 0.8 $\mathrm{GeV/c^2}$ (the maximum mass value found in the Monte Carlo simulation of reaction (1)). The acoplanarity distribution is shown in Fig. 4a with the events of Runs I and II summed together. A prominent peak at $\Delta\phi \sim 0°$ is noted in the data[1]. A similar peak is also seen in the Monte Carlo simulation of reaction (1), shown as a shaded histogram in Fig. 4b. This peak, however, is not seen in the separated beam data in Fig. 4c (solid histogram), nor in the distribution for events excluded in the visual scan shown in Fig. 4d, nor in the normalized background distribution[2] of reactions (2) in Fig. 4e. This peak is interpreted as evidence for exclusive production of a state decaying into two photons, as in reaction (1).

To obtain a background subtracted η signal, the $\Delta\phi$ distribution was divided into two regions: $0° - 4°$ where the η signal is dominant over background, and $4° - 20°$ where the background is dominant. The effect of the $\Delta\phi = 0° - 4°$ interval selection in reducing background can be seen in Fig. 2, where the corresponding $p_\perp^2$ distribution for the $\gamma\gamma$ system is shown as a shaded histogram. Compared to the $p_\perp^2$ distribution in the $0° - 20°$ interval, it is noticeably more peaked towards low values, as expected for events of reaction (1). The mass distribution of all events in the $0° - 4°$ interval is given by the shaded histogram in Fig. 3. It shows a narrower and more centered η signal than

[1] The regular structure seen in this distribution reflects the lead glass counter size of $\sim 4°$ in azimuth ϕ.

[2] For the normalization, the average values for $\Gamma_{\eta' \to \gamma\gamma}$, $\Gamma_{f \to \gamma\gamma}$ and $\Gamma_{A_2 \to \gamma\gamma}$ of Ref. 10 were used.

that seen in the mass distribution for the $0° - 20°$ interval. The numbers of events in the $0° - 4°$ and $4° - 20°$ intervals are given in Table 1 for the data samples of Runs I, II, and III, together with the corresponding numbers for the Monte Carlo simulations of reaction (1) and reactions (2).

We now evaluate the number of beam-gas events to be subtracted as background in the interval $0° - 4°$. The magnitude of this background is estimated using the separated beam data, normalized to the colliding beam data by the relation

$$\frac{N_d(0° - 4°) - B \cdot N_{bg}(0° - 4°)}{N_{MC}(0° - 4°)} = \frac{N_d(4° - 20°) - B \cdot N_{bg}(4° - 20°)}{N_{MC}(4° - 20°)} \tag{3}$$

Here the values in parentheses specify the $\Delta\phi$ angular region covered. N_d is the number of events in the given $\Delta\phi$ region for the colliding beam data sample (Fig. 4a), with the normalized contributions of reactions (2) (Fig. 4e) subtracted. N_{bg} and N_{MC} are the numbers of events for the beam-gas events from the separated beam data (Fig. 4c) and for the Monte Carlo simulation of reaction (1), respectively. B is the required normalization factor. The values of B determined from relation (3) for Run I and II are given in Table 1[1]. The background subtraction for both runs is small in the signal interval $0° - 4°$. The average level of the normalized background, plotted in larger angular intervals, is shown in Fig. 4c as a dashed line histogram. The numbers of events ascribed to reaction (1) in the signal interval $0° - 4°$, after subtraction of the normalized beam-gas background and the background from reactions (2), are given in Table 1 for Run I and II, respectively.

The cross section for reaction (1) can be written[11,12]

$$d\sigma(e^+e^- \to e^+e^-\eta) = \frac{\alpha^2}{16\pi^4 E_b \sqrt{E_b^2 - m_e^2}} \cdot \frac{d^3k_1' d^3k_2'}{E_1' E_2'} \cdot \frac{1}{q_1^2 q_2^2} \cdot W_{TT} \cdot K_{TT} \tag{4}$$

where k_1', E_1' and k_2', E_2' are the 3-momenta and energies of the scattered electrons, E_b is the beam energy and q_1 and q_2 are the 4-vectors of the virtual photons. K_{TT} contains the density matrix elements for the transversely polarized, virtual photons and is given by formula (29d) in Ref. 11. The function W_{TT} is given by[2]

$$W_{TT}(s, q_1^2, q_2^2) = \frac{\pi}{2} \cdot (\nu^2 - m_\eta^2 Q^2) \cdot F_\eta^2(q_1^2, q_2^2) \cdot \delta(s - m_\eta^2) \tag{5}$$

where s is the squared $\gamma\gamma$ CM energy, $Q = \frac{1}{2}(q_1 - q_2)$ and $\nu = Q\ (q_1 + q_2)$. The factor containing ν and Q results from the coupling of the photons to the pseudoscalar η meson [13]. F_η is the η form-factor. Its q^2-dependence was assumed to be that of a simple ρ-pole[3], i.e. F_η^2 is given by

$$F_\eta^2(q_1^2, q_2^2) = \frac{\Gamma_{\eta\to\gamma\gamma} \cdot 64\pi}{m_\eta^3} \cdot \left(1 - \frac{q_1^2}{m_\rho^2}\right)^{-2} \left(1 - \frac{q_2^2}{m_\rho^2}\right)^{-2}. \tag{6}$$

The radiative width $\Gamma_{\eta\to\gamma\gamma}$ can be expressed as

$$\Gamma_{\eta\to\gamma\gamma} = \frac{\sigma(e^+e^- \to e^+e^-\eta)}{I} \tag{7}$$

[1] The same separated beam data (taken with Run I trigger conditions) were used to determine the background subtraction for both Run I and II, i.e. we assume that the shape of the $\Delta\phi$ distribution of beam-gas events does not change from Run I to Run II. This is a reasonable, although unverifiable, assumption.

[2] W_{TT} can also be expressed as[12] $2\sqrt{X} \cdot \sigma_{TT}$, where $X = (q_1 q_2)^2 - q_1^2 q_2^2$. In the limit $q_1^2 \to 0, q_2^2 \to 0$, $\sigma_{TT} \to \sigma_{\gamma\gamma}$, the cross section for two real photons forming an η. $\sqrt{X}$ can then be interpreted as a flux factor.

[3] This assumption is motivated by the recent measurement of the q^2-dependence of η' production in the reaction $e^+e^- \to e^+e^-\eta'$[14].

where I is the result of the integration of (4), using (5) and (6) with $\Gamma_{\eta\to\gamma\gamma}$ set equal to 1. For the integration we used the computer program described in Ref. 15, which also yields 4-vector events of reaction (1). The final state particles of the simulated events were passed through a computer program which simulated the response of the various detector components, as well as known inefficiencies of the detector. For photons a program which simulates the electromagnetic shower development in the lead glass and in the material in front of it was used[16,17]. Finally, the simulated events were passed through the same analysis program and subjected to the same selection criteria as the real events.

The validity of the Monte Carlo simulation can be judged by a comparison of the distributions of the experimental data and the normalized Monte Carlo data. In Fig. 2 the observed $p_\perp^2$ distribution for the $\Delta\phi$ interval $0° - 4°$ (shaded histogram) can be compared with the normalized simulation result (continuous curve) and good agreement is seen. Note that the background of approximately 50 events was not subtracted in this figure. In the case of the $\Delta\phi$ distribution, the fully background subtracted data are shown along with the normalized simulation result in Fig. 4b. Good agreement is again seen, including the structure between 0° and 8° in $\Delta\phi$. At higher values of $\Delta\phi$ where statistics are poor, the value shown is the average over a 12° interval. Finally, in Fig. 5, the invariant mass distribution with the beam-gas background subtracted is shown together with the normalized Monte Carlo distribution for reaction (1). The contribution from reactions (2), mainly at masses above 0.8 GeV/c^2, is indicated with a dotted curve. The agreement is excellent[1]. For the purpose of subtracting the beam-gas background bin-by-bin, the shape of the beam-gas mass distribution in the $\Delta\phi$ interval $0° - 4°$ was assumed to be the same as that of the mass distribution for the beam-gas data in the $0° - 20°$ interval as shown by the solid histogram in Fig. 3.

The detection efficiency was obtained using the Monte Carlo simulation as described above. The curves of Fig. 1 were used in the simulation of the trigger efficiency. Corrections for the random occurrence of TOF counter signals (used as a veto in the trigger) were also applied. These corrections were 16.9 % for Run I and 14.6 % for Run II. The overall detection efficiencies for Run I and II are given in Table 1.

The cross section for reaction (1), $\sigma(e^+e^- \to e^+e^-\eta)$, was calculated from the number of background subtracted events, the detection efficiency, the integrated e^+e^- luminosity and the branching ratio $B(\eta \to \gamma\gamma) = 0.390 \pm 0.008$ [18]. The radiative width, $\Gamma_{\eta\to\gamma\gamma}$, was then calculated using relation (7). The results for Runs I and II are listed in Table 1. The two results are in good agreement and the weighted mean is $\Gamma_{\eta\to\gamma\gamma} = 0.53 \pm 0.04$ keV.

Systematic errors result from uncertainties in determining the e^+e^- integrated luminosity ($\pm$ 2.5 %), from the trigger efficiency simulation ($\pm$5 %), from the correction of the trigger efficiency for random TOF occurrence ($\pm$1 %), as well as from uncertainties in the detector simulation ($\pm$3 %). The latter systematic error comes mainly from the uncertainty in the conversion probability for photons in the material before the lead glass. The systematic error from the beam-gas background subtraction is estimated to be small.

Additional systematic errors may come from the integration procedure. The integration of relation (4) was limited to electron scattering angles of less than 35 mrad, since the small angle tagging detectors start at this angle and there are no tagged events in the data. Monte Carlo studies show that these scattering angles are smaller than 15 mrad when $p_\perp < 0.12$ GeV/c and $\Delta\phi = 0° - 4°$. However, using other angular limits in the integration changes $\Gamma_{\eta\to\gamma\gamma}$ by amounts which are smaller than the statistical precision of the Monte Carlo sample. Another systematic uncertainty stems from the assumed q^2-dependence in (6), since the q^2-dependence of the form-factor $F_\eta(q_1^2, q_2^2)$ is not known. Replacing the present assumption of ρ-pole q^2-dependence with a q^2-dependence obtained by squaring the ρ-poles, or with the q^2-dependence of a generalized VDM form-factor [19] changes $\Gamma_{\eta\to\gamma\gamma}$ by amounts smaller

[1]The main contribution above 0.8 GeV/c^2 comes from the decay $\eta' \to \gamma\gamma$. Indeed, after subtraction of the f and A_2 contributions, the data in the interval 0.80 – 1.12 GeV/c^2 give the corresponding width $\Gamma_{\eta'\to\gamma\gamma} = 4.0 \pm 0.9$ keV (statistical error only), in good agreement with the world average value[10] of $\Gamma_{\eta'\to\gamma\gamma} = 4.42 \pm 0.34$ keV.

than or comparable with the statistical precision ($\sim 2-4\%$) of the Monte Carlo samples. Thus we estimate that reasonable variations of the q^2-dependence in (6) should cause less than a 5 % change in the value of $\Gamma_{\eta\to\gamma\gamma}$.

Adding all of the above contributions in quadrature, we obtain a total systematic error of 8 % and thus

$$\Gamma_{\eta\to\gamma\gamma} = 0.53 \pm 0.04 \pm 0.04 \text{ keV}$$

The corresponding total width of the η meson is $\Gamma_\eta = 1.37 \pm 0.11 \pm 0.11$ keV.

The η radiative width $\Gamma_{\eta\to\gamma\gamma}$ obtained in this experiment is inconsistent with the result reported by A. Browman et al.[6] of $\Gamma_{\eta\to\gamma\gamma} = 0.324 \pm 0.046$ keV at a significance level of > 99 % ($\sim 3\sigma$), and with the earlier result of C. Bemporad et al.[6] of 1.00 ± 0.22 keV at a significance level of 96 % ($\sim 2\sigma$). Both of these experiments utilized the Primakoff effect in photoproduction and depend on the (theoretical) estimate of the nuclear electromagnetic form-factor and η production in the nuclear hadronic field. Our value is, however, in good agreement with the recent result of A. Weinstein et al.[8] of $0.56 \pm 0.12 \pm 0.10$ keV, which was also obtained in an e^+e^- storage ring experiment.

The $\gamma\gamma$ widths of the three neutral members of the pseudoscalar SU(3) nonet can be naively related as follows[20]:

$$\begin{aligned}\Gamma_{\eta\to\gamma\gamma} &= \tfrac{1}{3}\left(\frac{m_\eta}{m_{\pi^0}}\right)^3 \Gamma_{\pi^0\to\gamma\gamma}\left(\sqrt{8}\, r\sin\theta - \cos\theta\right)^2 \\ \Gamma_{\eta'\to\gamma\gamma} &= \tfrac{1}{3}\left(\frac{m_{\eta'}}{m_{\pi^0}}\right)^3 \Gamma_{\pi^0\to\gamma\gamma}\left(\sin\theta + \sqrt{8}\, r\cos\theta\right)^2\end{aligned} \tag{8}$$

Here θ is the SU(3) octet-singlet mixing angle and r is the ratio of singlet and octet spatial wave functions at the origin. Using our value for $\Gamma_{\eta\to\gamma\gamma}$, the value $\Gamma_{\pi^0\to\gamma\gamma} = 7.25 \pm 0.21$ eV[1] and the average value $\Gamma_{\eta'\to\gamma\gamma} = 4.42 \pm 0.34$ keV[10], we solve for r and θ and obtain

$$\begin{aligned} r &= 0.96 \pm 0.03 \\ \theta &= -18.4^\circ \pm 2.0^\circ \end{aligned}$$

This result is in good agreement with nonet symmetry ($r = 1$). The value of the mixing angle can be compared to the value from the quadratic mass formula[18], $\theta = -10^\circ$, or to a QCD calculation[21] giving $\theta = -17^\circ$ to -20°. In a study of the reaction $\pi^- p \to \eta' n$ [22], a value of $\theta = -16^\circ \pm 2^\circ$ was found.

We are indebted to the PETRA machine group and to the group of the DESY Computer Center for their excellent support during the experiment and to all engineers and technicians of the collaborating institutions who have participated in the maintenance of the apparatus. We express our thanks to F. Gutbrod and M. Poppe for helpful discussions. This experiment was supported by the Bundesministerium für Forschung und Technologie, by the Ministry of Education, Science and Culture of Japan, by the UK Science and Engineering Research Council through the Rutherford Appleton Laboratory and by the US Department of Energy. The visiting groups at DESY wish to thank the DESY directorate for the hospitality extended to them.

[1] This value corresponds to $\tau_{\pi^0} = (0.897 \pm 0.022 \pm 0.014) \cdot 10^{-16}$ sec.; J.W. Cronin[4].

REFERENCES

1. S. Matsuda and S. Oneda, Phys. Rev. **187** (1969), p. 2107.

   S. Okubo, in Symmetries and Quark Models, ed. R. Chand (1970), Gordon & Breach, New York.

   A. Kotlewski et al., Phys. Rev. **8** (1973), p. 348.

   A. Bramon and M. Greco, Phys. Lett. **48B** (1974), p. 137.

   F. Gault et al., Nuovo Cim. **24A** (1974), p. 259.

   Etim-Etim and M. Greco, Nuovo Cim. **42** (1977), p. 124.

   V.M. Budnev and A.E. Kaloshin, Phys. Lett. **66B** (1979), p. 351.

   S. Oneda and K. Terasaki, to be published in Supplements of Prog. Theor. Phys..

2. H. Suura, T.F. Walsh and B.-L. Young, Lett. Nuovo Cim. **4** (1972), p. 505.

   M.S. Chanowitz, Phys.Rev. Lett. **15** (1975), p. 977; Phys.Rev. Lett. **44** (1980), p. 59.

3. An extensive list of references can be found in Ref. 38 in J. Olsson, Proceedings of the Vth Intern. Workshop on Photon-Photon Collisions, Aachen 1983, Springer Lecture Notes in Physics Vol. 191.

4. G. von Dardel et al., Phys. Lett. **4** (1963), p. 51.

   G. Bellettini et al., Nuovo Cim. **40A** (1965), p. 1139; Nuovo Cim. **66A** (1970), p. 243.

   V.I. Kryshkin et al., JETP **30** (1970), p. 1037.

   A. Browman et al., Phys. Rev. Lett. **33** (1974), p. 1400.

   J.W. Cronin, Private communication.

5. D. Binnie et al., Phys. Lett. **83B** (1979), p. 141.

   Mark II Coll., G. Abrams et al., Phys. Rev. Lett. **43** (1979), p. 477.

   Cello Coll., H.J. Behrend et al., Phys. Lett. **114B** (1982), p. 378;
   Erratum, Phys. Lett. **125B** (1983), p. 518.

   Jade Coll., W. Bartel et al., Phys. Lett. **113B** (1982), p. 190.

   Mark II Coll., P. Jenni et al., Phys. Rev. **D27** (1983), p. 1031.

   Pluto Coll., Ch. Berger et al., Phys. Lett. **142B** (1984), p. 125.

   Tasso Coll., M. Althoff et al., Phys. Lett. **147B** (1984), p. 487.

6. C. Bemporad et al., Phys. Lett. **25B** (1967), p. 380.

   A. Browman et al., Phys. Rev. Lett. **32** (1974), p. 1067.

7. H. Primakoff, Phys. Rev. **81** (1951), p. 899.

8. A. Weinstein et al., Phys. Rev. **D28** (1983), p. 2896.

9. Jade Coll., W. Bartel et al., Phys. Lett. **88B** (1979), p. 171; Phys. Lett. **92B** (1980), p. 206;
   Phys. Lett. **99B** (1981), p. 277.

10. A. Cordier, Proceedings of the VIth Intern. Workshop on Photon-Photon Collisions, Lake Tahoe, USA, 1984.

11. G. Bonneau, M. Gourdin and F. Martin, Nucl. Phys. **B54** (1973), p. 573.

12. V.M. Budnev et al., Phys. Rep. **15c4** (1975), p. 181.

13. G. Köpp, T.F. Walsh and P. Zerwas, Nucl. Phys. **B70** (1974), p. 461.

14. Pluto Coll., Ch. Berger et al., in ref. 5.

15. S. Kawabata, Program Write-up, unpubl. (1982).

ibid., Contribution to the parallel sessions, reported by J.H. Field, Proceedings of the IVth Intern. Colloquium on Photon-Photon Interactions, Paris 1981, p. 447.

16. H. Messel and D.F. Crawford, Electron-Photon Shower Distribution Function Tables, Pergamon Press, 1970.

A. Sato, Master's Thesis, Tokyo University 1978, unpubl.

17. Jade Coll., W. Bartel et al., in ref. 5.

18. Particle Data Group, Rev. Mod. Phys. **56** (1984), p. 51.

19. I.F. Ginzburg and V.G. Serbo, Phys. Lett. **109B** (1982), p. 231.

20. see, e.g., J.H. Field, Proceedings of the Intern. Europhysics Conf. on High Energy Physics, Brighton, UK, 1983.

21. A.T. Filippov, Sov. J. Nucl. Phys. **29** (1979), p. 534.

22. W.D. Apel, Sov. J. Nucl. Phys. **25** (1977), p. 300.

FIGURE CAPTIONS

Figure 1 Trigger signal efficiency of lead glass counter septants as a function of detected energy, for Low Threshold operation (continuous curve) and for High Threshold operation (dashed curve).

Figure 2 The distribution of $p_\perp^2$ of the $\gamma\gamma$ system relative to the beam, for all events of Runs I and II passing the selection criteria i) through vii). The shaded histogram shows the same distribution with the additional requirement on acoplanarity: $\Delta\phi = 0° - 4°$. The continuous curve shows the Monte Carlo simulation result (see text).

Figure 3 Invariant $\gamma\gamma$ mass distribution for all events of Runs I and II passing the selection criteria i) through viii). The shaded histogram shows the mass spectrum with the additional requirement on acoplanarity: $\Delta\phi = 0° - 4°$. The solid histogram shows the mass distribution for separated beam events (Run III) passing selection criteria i) – viii).

Figure 4 The distribution of acoplanarity angle $\Delta\phi$ for events with $m(\gamma\gamma) < 0.8$ GeV/c^2, selected with criteria i) – viii): a) for events of Runs I and II, b) for fully background subtracted Run I and II data with the shaded histogram showing the normalized Monte Carlo simulation result, c) for events of Run III with separated beams (solid histogram) and for the normalized distribution calculated with the factor B (dashed line histogram, see text), d) for events excluded in the visual scan and e) for the normalized background from other beam-beam interactions (reactions (2)) from Monte Carlo simulation.

Figure 5 Invariant $\gamma\gamma$ mass distribution for events of Runs I and II selected with criteria i) – viii) for the angular interval $\Delta\phi = 0° - 4°$, with beam-gas background subtracted. Data are shown with a continuous line histogram. The Monte Carlo simulation for reaction (1) and for reactions (2) are shown as a continuous curve and as a dotted curve, respectively.

Table 1

DETERMINATION OF $\Gamma_{\eta\to\gamma\gamma}$			
Trigger Condition	Low Threshold		High Threshold
Data Sample	Run I	Run III sep. beams	Run II
Integrated luminosity (pb^{-1})	17.1	–	14.6
Selected event sample	888	30	585
Selected event sample with $m(\gamma\gamma) < 0.8$ GeV/c^2			
$\Delta\phi = 0° - 4°$	271	2	224
$\Delta\phi = 4° - 20°$	562	28	316
Monte Carlo event sample[1] (reaction (1))			
$\Delta\phi = 0° - 4°$	3996	–	3100
$\Delta\phi = 4° - 20°$	1654	–	1501
Monte Carlo event sample with $m(\gamma\gamma) < 0.8$ GeV/c^2 (reactions (2), normalized)			
$\Delta\phi = 0° - 4°$	3.4	–	2.9
$\Delta\phi = 4° - 20°$	7.8	–	6.8
Beam-gas background subtraction factor B	15.7 ± 3.2	–	7.5 ± 1.6
Selected event sample, with $m(\gamma\gamma) < 0.8$ GeV/c^2, background subtracted			
$\Delta\phi = 0° - 4°$	236.2 ± 29.3	–	206.1 ± 19.2
Detection efficiency[2] (%)	2.62 ± 0.05	–	2.46 ± 0.05
$\sigma(e^+e^- \to e^+e^-\eta)$[2], nb	1.35 ± 0.17	–	1.48 ± 0.14
$\Gamma_{\eta\to\gamma\gamma}$, keV	0.506 ± 0.064	–	0.554 ± 0.054
$\Gamma_{\eta\to\gamma\gamma}$, weighted average, keV	0.534 ± 0.041		

[1] There are no events with $m(\gamma\gamma) > 0.8$ GeV/c^2.

[2] These values are calculated for electron scattering angles < 55 mrad.

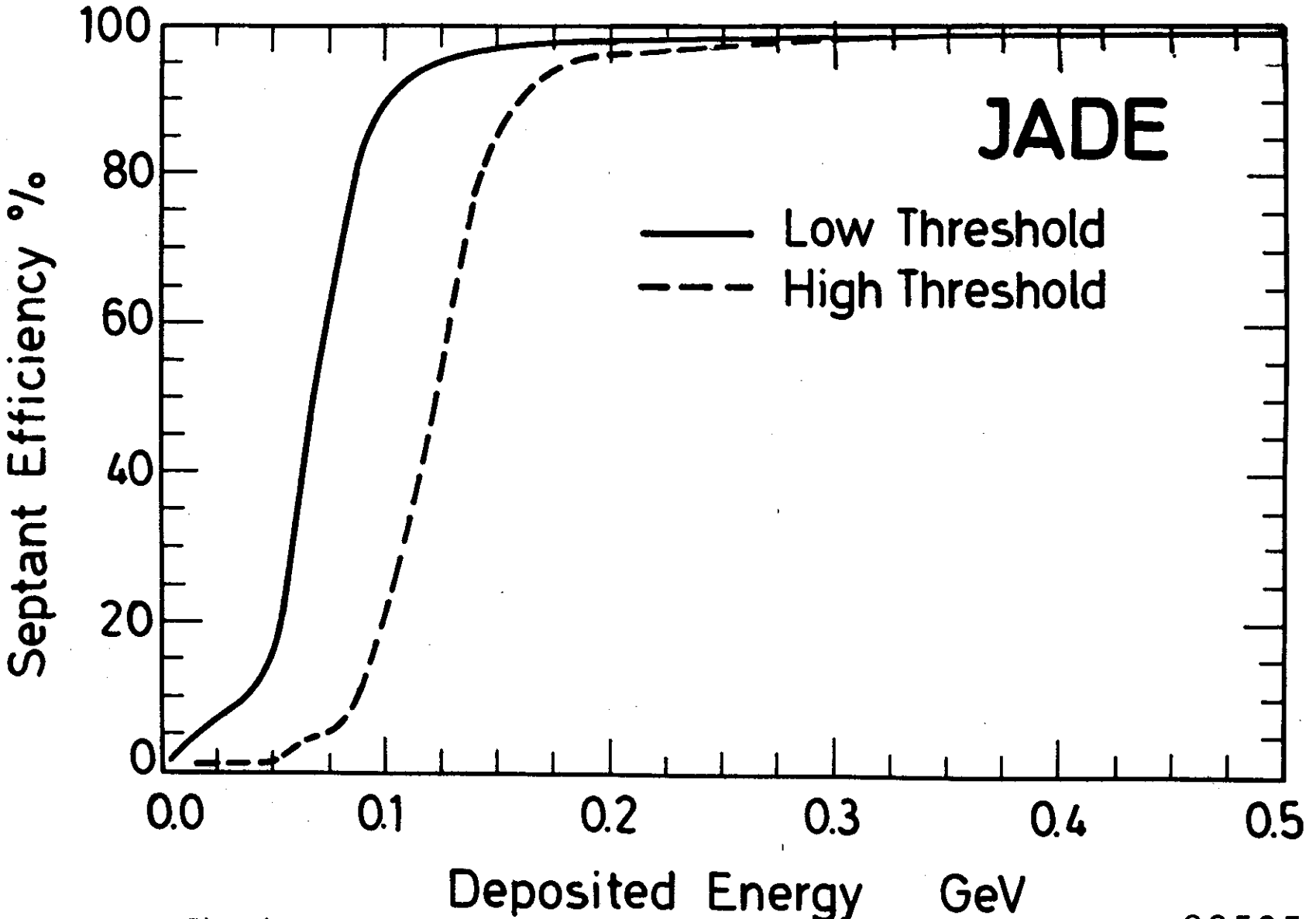
JADE
Low Threshold
High Threshold
Septant Efficiency %
100
80
60
40
20
0
0.0
0.1
0.2
0.3
0.4
0.5
Deposited Energy GeV
38505

Fig. 1

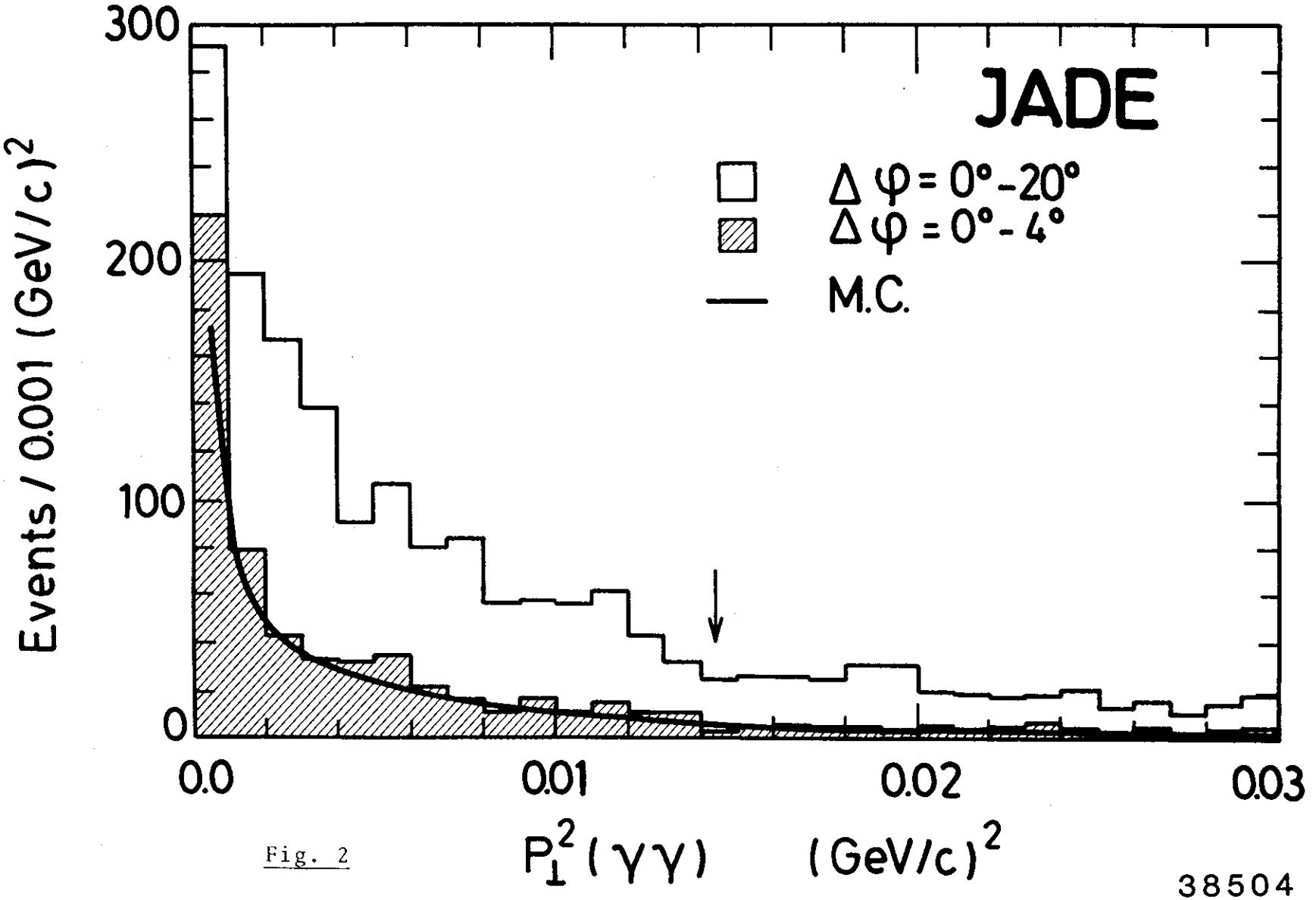
JADE
Δφ = 0°-20°
Δφ = 0°-4°
M.C.
Events / 0.001 (GeV/c)²
300
200
100
0
0.0
0.01
0.02
0.03
P⊥²(γγ) (GeV/c)²
38504

Fig. 2

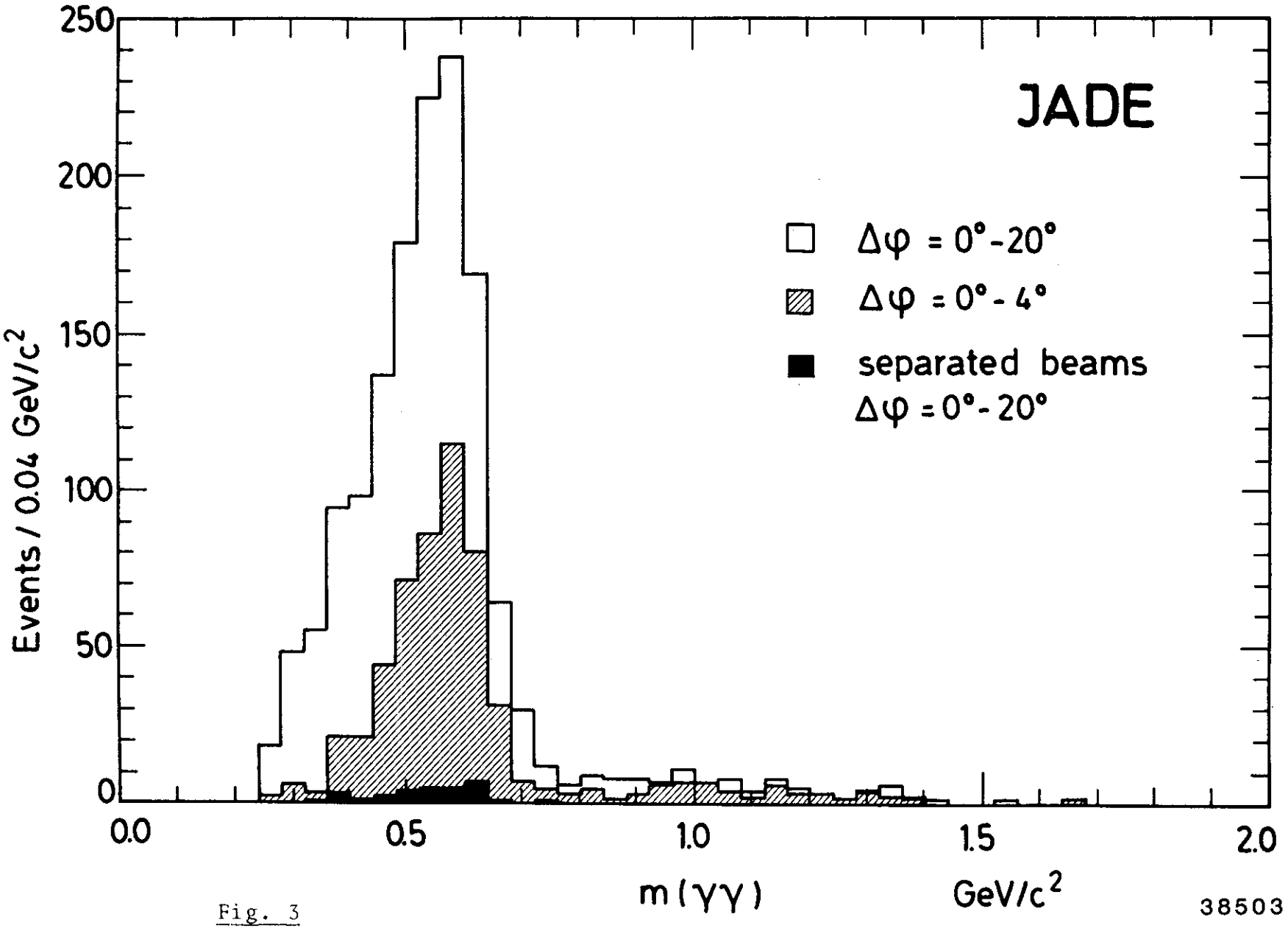
JADE
Δφ = 0°-20°
Δφ = 0°- 4°
separated beams
Δφ = 0°- 20°
Events / 0.04 GeV/c²
m(γγ) GeV/c²
0
50
100
150
200
250
0.0
0.5
1.0
1.5
2.0
38503

Fig. 3

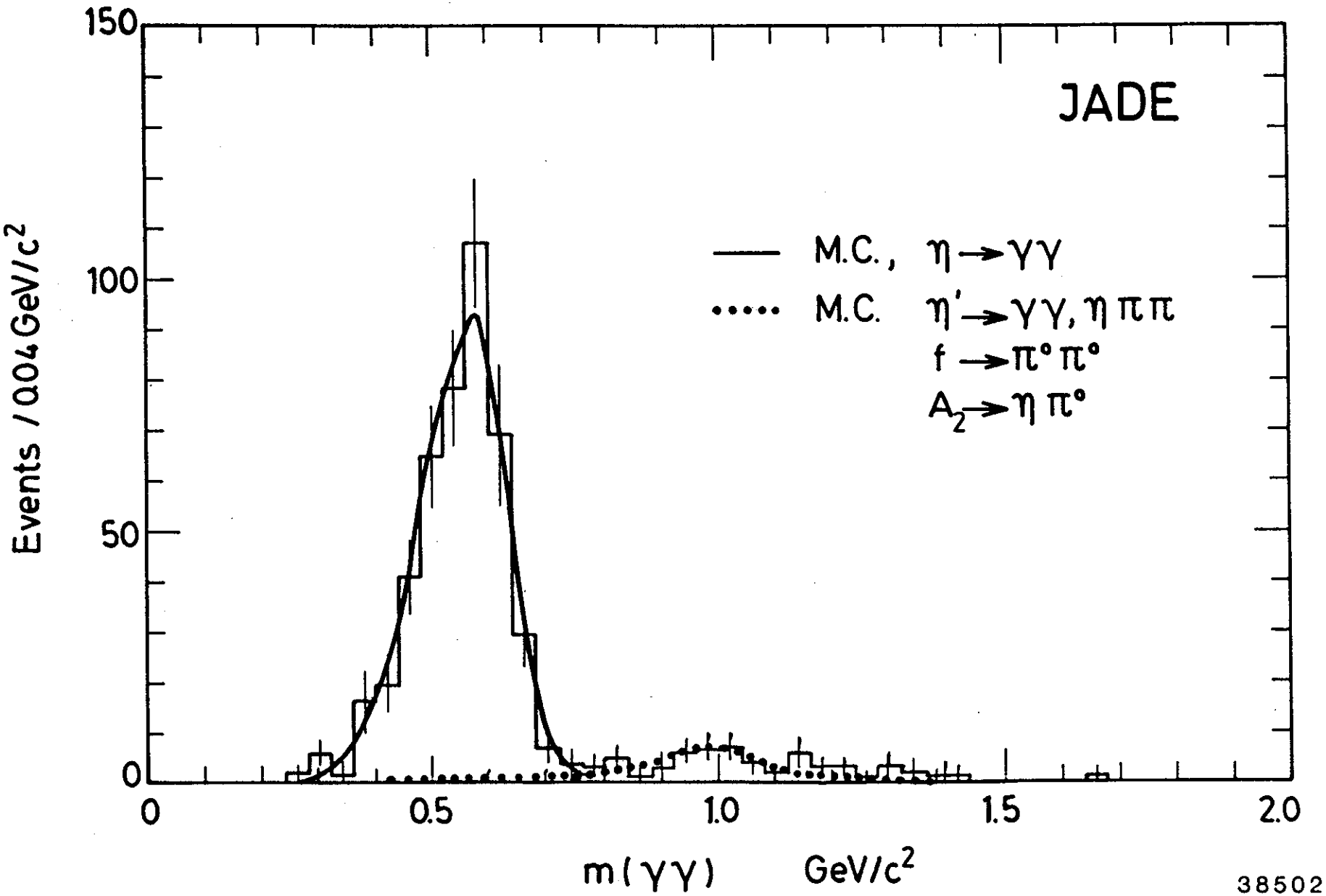
JADE
M.C., η → γγ
M.C. η' → γγ, η π π
f → π° π°
A2 → η π°
Events /0.04 GeV/c²
m(γγ) GeV/c²
150
100
50
0
0
0.5
1.0
1.5
2.0
38502

Fig. 5

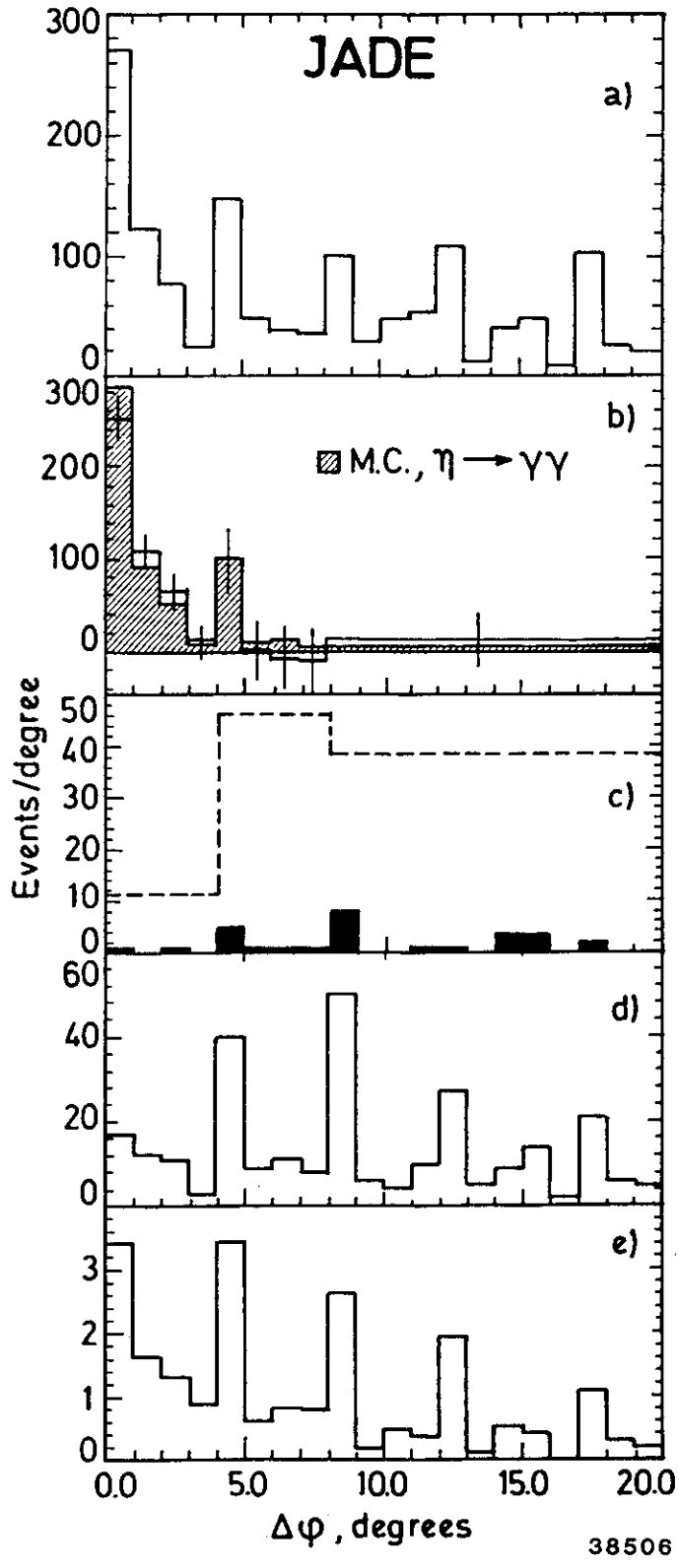

Fig. 4